NJC

ROYAL SOCIETY OF CHEMISTRY

PAPER

View Article Online
View Journal | View Issue

Cite this: *New J. Chem.*, 2024, **48**, 20140

Structures and properties of the mono- and diprotonated species of acetylenedicarbonyl fluoride†

Dirk Hollenwäger, * Alexander Nitzer, Dominik Leitz and Andreas J. Kornath‡

Received 24th September 2024,
Accepted 17th November 2024

DOI: 10.1039/d4nj04175e

rsc.li/njc

In this study, the first crystal structure of acetylenedicarbonyl fluoride is reported. Furthermore, the title compound was investigated in the superacidic media XF/SbF_5 (X = H, D) which led to the formation of the monoprotonated species. Sur-prisingly, the diprotonated species was only formed by employing the monoprotonated species in 1,1,1,2-tetrafluoroethane whereas attempts at its synthesis in anhydrous hydrogen fluoride were unsuccessful. The vibrational spectroscopy is discussed together with quantum chemical calculations on the DFT/aug-cc-pVTZ level of theory. The stability of the *Z*-conformation of protonated acyl fluorides is calculated on the MP2/aug-cc-pVTZ level of theory.

Introduction

Acid fluorides are often prepared from their chlorides. *Via* the synthetic route of metathesis, a chlorine–fluorine exchange is often explored with antimony fluorides, less commonly with aHF.[1] Acetylenedicarbonyl chloride can be obtained by the decomposition of an anthracene derivative as the starting material.[2] The metathesis for acetylenedicarbonyl fluoride is not ecologically or economically viable due to the low yield of acetylenedicarbonyl chloride.[2] The direct synthesis of acetylenedicarbonyl chloride starting with acetylenedicarboxylic acid with classical chlorinating agents reacts after removal of the solvent to the addition product with added HCl (PCl_5, $POCl_3$) or Cl_2 ($SOCl_2$) at the triple bond.[3,4] The acetylenedicarbonyl fluoride is the best-known structure compared to the corresponding acetylenedicarbonyl halides. One of the most efficient reaction pathways to obtain acetylenedicarbonyl fluoride is the use of sulfur tetrafluoride.[5] The first synthesis was reported in 1960 by Hasek.[5] In 1973, the synthesis of acetylenedicarbonyl fluoride was optimised and supplemented by the synthesis using the potassium salt of the carboxylic acid as starting material.[5,6] Although its synthesis is reported in the literature, many properties are still unknown. Acetylenedicarbonyl fluoride was investigated in CCl_4 solution in Raman and ^{19}F NMR spectroscopy (49.2 ppm) in 1973.[6] The Raman spectrum is only described by the stretching oscillation of C–F (1822 cm^{-1}) and C≡C (2262 cm^{-1}).[6] In 1975, the pure substance was only characterized by its mass spectrum, vapor pressure, boiling (46 °C), and melting point (−51 °C).[7] In summary, compared to other acid fluorides, acetylenedicarbonyl fluoride is rarely described in the literature, and its basicity remains unknown. Additionally, the investigations of protonated acyl fluorides are very rare. Only five crystal structures are known from protonated acyl fluorides the haloacetyl fluorides, dichloroacetyl fluoride, and fumaryl fluoride.[8–10] This prompted us to investigate acetylenedicarbonyl fluoride in superacidic media.

Results and discussion

Synthesis and properties of $[C_4(OH)OF_2][SbF_6]$ (2) and $[C_4(OD)OF_2][SbF_6]$ (3)

The monoprotonated species of acetylenedicarbonyl fluoride is obtained in the superacidic system HF/SbF_5, using anhydrous hydrogen fluoride (aHF), or aDF for deuterated salts, as reagent and solvent (eqn (1)). The salts are soluble in aHF and grew as colourless crystals in solution. The salts of **2** and **3** are stable up to −43 °C. The solvent was removed overnight at −78 °C.

1 X = H (**2**), D (**3**) (1)

Synthesis and properties of $[C_4(OH)_2F_2][Sb_2F_{11}]_2 \cdot 2HF$ (4) $[C_4(OD)_2F_2][Sb_2F_{11}]_2 \cdot 2HF$ (5)

The salts of diprotonated species **4** and **5** are prepared from the corresponding salts of the monoprotonated species (**2** resp. **3**).

Department Chemie, Ludwig-Maximilians-Universität München, Butenandtstr. 5–13, 81377 Munich, Germany. E-mail: Dirk.Hollenwaeger@cup.uni-muenchen.de

† Electronic supplementary information (ESI) available. CCDC 2371787, 2371788 and 2371790. For ESI and crystallographic data in CIF or other electronic format see DOI: https://doi.org/10.1039/d4nj04175e

‡ Prof. Dr Andreas J. Kornath passed away in March 2024.

The salts (**2** and **3**) decompose when mixed with an excess of SbF_5 in the aprotic solvent 1,1,1,2-tetrafluoroethane (R-134a) at −25 °C over a period of 25 minutes. The decomposition results in the formation of the starting material (**1**) and salts of the diprotonated species are formed which is described in eqn (2). Salt containing the diprotonated species could not be obtained in anhydrous HF or deuterium fluoride even in the presence of 15 equivalents of SbF_5. Although the diprotonation can only occur by decomposition, the salts are stable in aHF and can be recrystallized. The products were obtained as yellowish salts stable up to 0 °C.

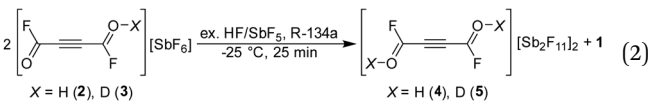

(2)

Vibrational spectroscopy

Vibrational spectroscopy of $C_4O_2F_2$ (1). The low (l.t.) and room temperature (r.t.) Raman and IR of $C_4O_2F_2$ (**1**) are illustrated in Fig. 1. In Table 1 selected observed Raman and IR frequencies of **1** are summarized together with the quantum chemically calculated frequencies of the $[C_4(OH)OF_2]^+ \cdot HF$ cation as well as their assignments. The complete analysis of the vibrational frequencies is provided in the ESI† in Table S1.

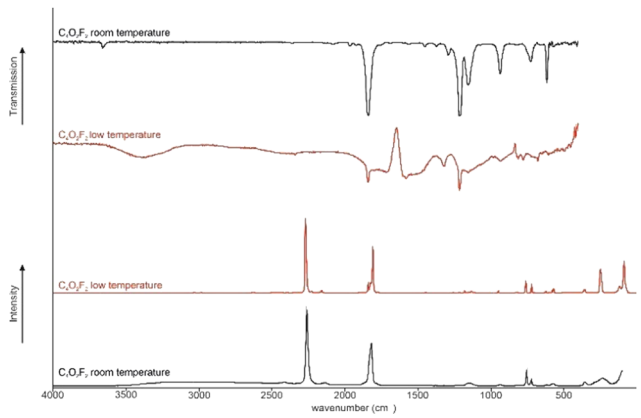

Fig. 1 Low-temperature Raman and IR spectra of $C_4O_2F_2$ (**1**).

The $C_4O_2F_2$ molecule possesses C_2 symmetry, whereby 18 fundamental vibrational modes are expected.

In fair agreement with the values reported in the literature, the C≡C stretching vibration is detected at 2263 cm^{-1} (r.t. Ra) and 2271 cm^{-1} (l.t. Ra,), respectively.[6] The C=O stretching vibrations are observed at 1842 cm^{-1} (IR) at both temperatures and. 1843 cm^{-1} (Ra) at low temperatures, respectively.[6] The symmetric C=O stretching vibration is detected at 1819 cm^{-1} (r.t. Ra) and at 1810 cm^{-1} (l.t. Ra), respectively. In comparison to FC(O)NCS (1854 cm^{-1}) the C=O stretching vibration is in the same range.[11] Compared to FC(O)SCN (1867 cm^{-1}) and $FC(O)SOC(O)CF_3$ (*trans* ap–sp: 1876 cm^{-1}) the C=O stretching vibration is red shifted.[11,12] The antisymmetric C–F oscillation is identified at 1215 cm^{-1} (IR) at both temperatures and 1179 cm^{-1} (l.t. Raman). The C–F stretching vibration is in the same range compared to FC(O)NCS (1245 cm^{-1}).[11] The symmetric C–F stretching vibration is detected at 1159 cm^{-1} (r.t. IR), 1150 cm^{-1} (l.t. Raman), 1155 cm^{-1} (r.t. IR) resp. 1133 cm^{-1} in Raman. Compared to the C–F stretching vibration of FC(O)NCS (1108 cm^{-1}) the oscillation is blue-shifted.[11] The antisymmetric C–C vibration is observed at room temperature in IR at 939 cm^{-1} (IR) and. 938 cm^{-1} (Ra) and at low at 935 cm^{-1} (IR) and. 950 cm^{-1} in (Ra). The antisymmetric C–C oscillation is identified at room temperature in Raman at 757 cm^{-1} and low temperature at 763 cm^{-1} (Ra) and 781 cm^{-1} (IR).

Vibrational spectroscopy of $[C_4(OH)OF_2][SbF_6]$ (2) and $[C_4(OD)OF_2][SbF_6]$ (3). The low-temperature Raman and IR spectra of $[C_4(OH)OXF_2][SbF_6]$ (**2**, **3**) (X = H, D) are illustrated in Fig. 2. In Table 2 selected observed Raman and IR frequencies of **2**, and **3** are listed together with the quantum chemically calculated frequencies of $[C_4(OH)OF_2]^+ \cdot HF$ cation as well as their assignments. The complete analysis of the vibrational frequencies is summarized in the ESI† in Table S2.

The monoprotonated species $[C_4(OH)OF_2]^+$ possesses C_1 symmetry with 21 expected fundamental vibrational modes, showing both Raman and IR activity. In comparison with the starting material, the monoprotonation has no influence on the C≡C bond, the unprotonated C=O bond, and the symmetric C–C stretching vibration. Clear evidence of a monoprotonation is the stretching vibration of the C=O bond, which is red-shifted in IR to 1653 cm^{-1} and in Ra at 151 cm^{-1} to 1659 cm^{-1}.

Table 1 Selected observed vibrational frequencies [cm^{-1}] of $C_4O_2F_2$ (**1**) and calculated vibrational frequencies [cm^{-1}] of $C_4O_2F_2$

1 at room temperature[a]		**1** at low temperature[a]					
IR	Ra	IR	Ra	ν (IR/Ra)[bc]	Assignment		
	2263 (100)		2271 (100)	2257 (0/515)	ν_1	A	ν_s(C≡C)
1842 (s)		1842 (s)	1843 (12)	1812 (578/19)	ν_{11}	B	ν_{as}(CO)
	1819 (57)		1810 (60)	1810 (190/172)	ν_2	A	ν_s(CO)
1215 (s)		1215 (vs)	1179 (2)	1183 (696/1)	ν_{12}	B	ν_{as}(CF)
1159 (s)	1150 (4)	1155 (s)	1133 (3)	1102 (174/14)	ν_3	A	ν_s(CF)
939 (m)	938 (2)	935 (m)	950 (3)	908 (122/3)	ν_{13}	B	ν_{as}(C–C)
	757 (21)	781 (m)	763 (16)	729 (12/8)	ν_4	A	ν_s(C–C)

[a] Abbreviations for IR intensities: vs = very strong, s = strong, m = medium, w = weak, sh = shoulder, br = broad. Experimental Raman intensities are relative to a scale of 1 to 100. [b] Calculated on the B3LYP/aug-cc-pVTZ level of theory. Scaling factor: 0.968. [c] IR intensities in km mol^{-1}; Raman intensities in $Å^4/u$.

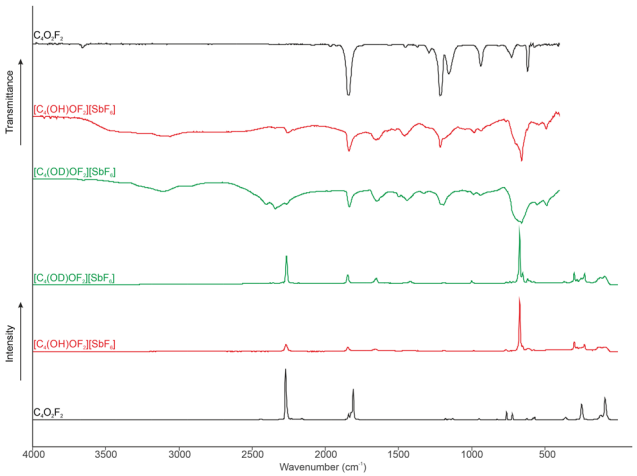

Fig. 2 Low-temperature Raman and IR spectra of $C_4O_2F_2$, **2**, and **3**.

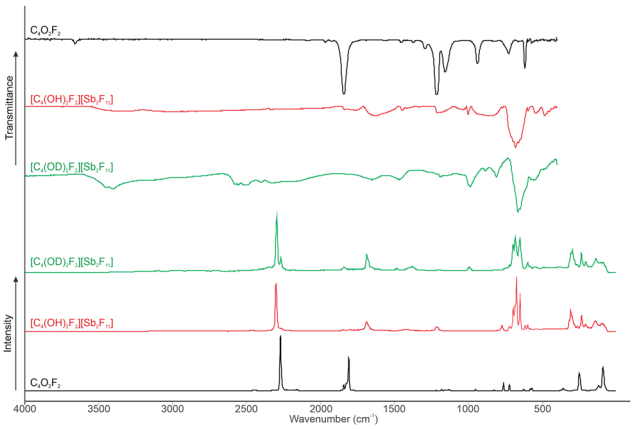

Fig. 3 Low-temperature Raman and IR spectra of $C_4O_2F_2$, **4**, and **5**.

Also, in IR the OH oscillation is identified at 3084 cm^{-1}. Furthermore, the protonation is detected by a blue shift of the C–F bond by 243 cm^{-1} in IR at 1458 cm^{-1} and in Ra at 1445 cm^{-1}. The antisymmetric stretching vibration is blue-shifted in IR and Ra to 986 cm^{-1}.

Vibrational spectroscopy of $[C_4(OH)_2F_2][Sb_2F_{11}]\cdot 2HF$ (4) and $[C_4(OD)_2F_2][Sb_2F_{11}]\cdot 2HF$ (5). The low-temperature Raman and IR spectra of $[C_4(OX)_2OF_2][Sb_2F_{11}]$ (X = H, D) (**4**, **5**) are illustrated in Fig. 3. In Table 3 are selected observed Raman and IR frequencies of **4** and **5** are listed together with the quantum chemically calculated frequencies of $[C_4(OH)OF_2]^+\cdot HF$ as well as their assignments. The complete analysis of the vibrational frequencies can be seen in the ESI† in Table S3. The diprotonated species $[C_4(OH)_2F_2]^+$ possesses C_{2h} symmetry with 24 expected fundamental vibrational modes. The diprotonation causes a slight effect on the C≡C by a blue shift of 37 cm^{-1} to 2300 cm^{-1}. Furthermore, after protonation the C≡C bond leads to a change of dipole moment which is not present in the starting material and is detected at 2334 cm^{-1} (IR). The C=O stretching vibrations are red-shifted and can be observed at 1626 cm^{-1} in IR and 1688 cm^{-1} in Ra. In IR the antisymmetric C–F bond is blue-shifted to 1445 cm^{-1} and the symmetric C–F bond to 1418 cm^{-1}. The effect on the C–C vibration is within the standard deviation.

Crystal structure

Crystal structure of $C_4O_2F_2$ (1). The starting material **1** crystallizes in the tetragonal space group $P4_12_12$ with four formula units per unit cell. Selected bond lengths, bond angles, dihedral angles and interatomic contacts are listed in Table 4. Further crystallographic data can be found in the ESI† (Chapter S2). The formula unit is displayed in Fig. 4 the C≡C bond length of 1.186(2) Å is in the expected range for an average triple bond (1.183 Å).[13] The C1–C2 bond of 1.445(2) Å and is slightly shortened compared to an average single carbon bond (1.466 Å) with a similar bonding situation. The C=O bond length of 1.178(2) Å is comparable to the corresponding bond lengths of malonyl difluoride (1.177(3) Å) and fumaryl fluoride (1.177(4) Å), respectively.[14,15] The C–F bond of **1** (1.332(1) Å) is significantly shortened compared to the C–F bond reported for malonyl difluoride (1.349(4) Å) and fumaryl fluoride (1.334(2) Å).[14,15] In **1** the molecules are connected *via* C···O donor–acceptor interactions. The molecules within one layer are connected by 3.078(2) Å interatomic contacts and the next layer is connected by 2.896 Å C···O contacts. The interatomic

Table 2 Selected observed vibrational frequencies [cm^{-1}] of $[C_4(OH)OF_2][SbF_6]$, $[C_4(OD)OF_2][SbF_6]$, and calculated vibrational frequencies [cm^{-1}] of $[C_4(OH)OF_2]^+\cdot HF$

2 exp.[a]		**3** exp.[a]		$[C_4(OH)OF_2]^+\cdot HF$ calc.[bc]			
IR	Ra	IR	Ra	IR/Ra	Assignment		
3084 (m)				2878 (2945/159)	ν_1	A	ν(OH)
2257 (m)	2269 (14)	2264 (m)	2264 (56)	2237 (490/425)	ν_2	A	ν(C≡C)
1840 (s)	1846 (9)	1838 (s)	1848 (20)	1823 (213/194)	ν_3	A	ν(CO)
1653 (m)	1659 (5)	1647 (m)	1654 (13)	1597 (634/37)	ν_4	A	ν(CO)
1458 (m)	1445 (2)	1443 (m)	1418 (6)	1422 (376/1)	ν_5	A	ν(CF)
		1194 (m)		1164 (324/26)	ν_7	A	ν(CF)
986 (m)	986 (2)	989 (m)	1000 (7)	963 (34/39)	ν_8	A	ν_{as}(C–C)
768 (w)	766 (4)		764 (6)	737 (12/7)	ν_{10}	A	ν_s(C–C)

[a] Abbreviations for IR intensities: vs = very strong, s = strong, m = medium, w = weak, sh = shoulder, br = broad. Experimental Raman intensities are relative to a scale of 1 to 100. [b] Calculated on the B3LYP/aug-cc-pVTZ level of theory. Scaling factor: 0.968. [c] IR intensities in km mol^{-1}; Raman intensities in $Å^4/u$.

Table 3 Selected observed vibrational frequencies [cm^{-1}] of $[C_4(OH)_2F_2][Sb_2F_{11}]_2$, $[C_4(OD)_2F_2][Sb_2F_{11}]_2$, and calculated vibrational frequencies [cm^{-1}] of $[C_4(HO)_2F_2]^{2+}\cdot 2HF$

4 exp.[a]		**5** exp.[a]		$[C_4(OH)_2F_2]^+\cdot HF$ calc.[bc]			
IR	Ra	IR	Ra	IR/Ra	Assignment		
		3446 (m)			ν_1	A	ν_s(OH)
2334 (s)	2300 (88)	2328 (m)	2296 (100)	2266 (24/843)	ν_2	A	ν(C≡C)
1626 (s)	1688 (18)	1649 (m)	1686 (32)	1659 (174/68)	ν_4	A	ν_s(CO)
		1635 (m)		1651 (1262/6)	ν_{15}	B	ν_{as}(CO)
1445 (s)		1472 (w)	1488 (7)	1422 (405/1)	ν_{16}	B	ν_{as}(CF)
1418 (s)			1382 (10)	1387 (298/35)	ν_5	A	ν_s(CF)
957 (s)		986 (m)	994 (9)	984 (163/1)	ν_{19}	B	ν_{as}(CC)
770 (vw)	772 (11)			762 (20/14)	ν_8	A	ν_s(CC)

[a] Abbreviations for IR intensities: vs = very strong, s = strong, m = medium, w = weak, sh = shoulder, br = broad. Experimental Raman intensities are relative to a scale of 1 to 100. [b] Calculated on the B3LYP/aug-cc-pVTZ level of theory. Scaling factor: 0.968. [c] IR intensities in km mol^{-1}; Raman intensities in $Å^4$/u.

Table 4 Selected bond lengths, interionic distances [Å] and bond angels [°] of 1 and symmetry codes: i = −x, −y, −z; ii = −0.5 − x, 0.5 + y, −0.25 + z; iii = −1.5 − x, 0.5 + y, −0.25 + z

Bond lengths [Å]			
C1–C2	1.445(2)	C1–O1	1.178(2)
C2–C2^{i}	1.186(2)	C1–F1	1.332(1)
Bond angles [°]			
C1–C2–C2^{i}	177.9(1)	F1–C1–C2	111.3(1)
O1–C1–C2	126.7(1)	O1–C1–F1	121.9(1)
Intermolecular contacts [Å]			
O1···C1^{ii}	3.078(2)	O1···C1^{iii}	2.896(2)

Fig. 4 Formula unit of $C_4O_2F_2$ (displacement ellipsoids with 50% probability). Symmetry operation i = −x, −y, −z.

Table 5 Selected bond lengths, interionic distances [Å] and bond angels [°] of 2 and symmetry codes: i = 1 − x, 1 − y, −z; ii = 1 − x, 1 − y, 1 − z; iii = x, −1 + y, z; iv = 2 − x, −1 − y,1 − z

Bond lengths [Å]			
C1–C2	1.423(9)	C4–O2	1.174(8)
C2–C3	1.184(9)	C1–F1	1.289(5)
C3–C4	1.457(9)	C4–F2	1.321(7)
C1–O1	1.218(6)		
Bond angles [°]			
C1–C2–C3	176.5(6)	F1–C1–O1	120.6(5)
C2–C3–C4	176.5(6)	O2–C4–C3	125.1(5)
O1–C1–C2	122.9(5)	F2–C4–C3	111.8(5)
F1–C1–C2	116.4(5)	F2–C4–O2	123.1(5)
Intermolecular contacts [Å]			
O1–(H1)···F3	2.384(6)	C2–F8^{iii}	3.057(6)
C1–F7^{i}	2.711(7)	C3–F5^{iv}	3.064(5)
C1–F4^{ii}	2.942(6)	C4–F5^{iv}	2.754(4)

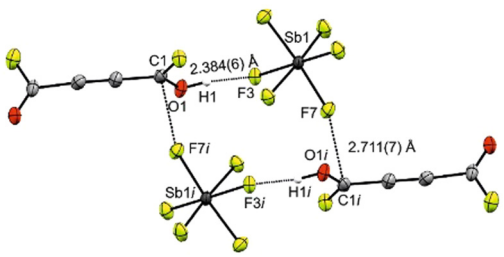

Fig. 5 Two formula units with intermolecular contacts and hydrogen bonds in the crystal structure of **2** (displacement ellipsoids with 50% probability). Symmetry codes: i = 2 − x, 1 − y, 1 − z.

contacs are 90% and 96% below the radii of the van-der-Waals radii. The distance is comparable to the contact of FC(O)···C(O)CF_3 (3.037 Å) and FC(O)···CF_3 (3.217 Å).[16]

Crystal structure of $[C_4(OH)OF_2][SbF_6]$ (2). The monoprotonated species of $C_4O_2F_2$ crystallizes in the triclinic space group $P\bar{1}$ with two formula units per unit cell. Selected bond lengths, bond angles, dihedral angles, and interatomic contacts are listed in Table 5. Further crystallographic data can be found in the ESI† (Chapter S2). Two formula units are displayed in Fig. 5 together with the intermolecular contacts.

In comparison with the starting material, the monoprotonation does not significantly affect the bond lengths of the unprotonated acyl fluoride moiety, the C3–C4 and the C≡C bond. The C1=O1 bond is significantly elongated by approximately 0.040 Å to 1.218(6) Å compared to the neutral compound. The C1–F1 bond (1.289(5) Å) is shortened by 0.043 Å compared to **1**. The Sb–F bond lengths of anion are in the range from 1.853(3) Å to 1.961(3) Å and in agreement with those reported in the literature.[17,18] Distorting the ideal O_h symmetry is caused by strong hydrogen bonds of O1–(H1)···F3 with a length of 2.384(6) Å. Also, the C–F interaction leads to a distortion of the ideal symmetry. The layer structure is built *via* the hydrogen bonds and the C1–F7 interatomic interaction. The layers are linked by four additional C–F interactions.

Crystal structure of $[C_4(OH)_2F_2][Sb_2F_{11}]\cdot 2HF$ (4). The diprotonated species of $C_4O_2F_2$ crystallizes in the triclinic space group $P\bar{1}$ with two formula units per unit cell. Selected bond lengths, bond angles, dihedral angles and interatomic contacts are listed in Table 6. Further crystallographic data can be found in the ESI† (Chapter S2). The formula unit of **3** is displayed in Fig. 6.

Compared to the neutral compound **1**, the C≡C is not affected by the protonation. The shortening of the C–C bond is

Table 6 Selected bond lengths, interionic distances [Å] and bond angels [°] of 4 and symmetry codes: i = 1 − x, 2 − y, −z, ii = 1 − x, 2 − y, 1 − z, iii = x, 1 + y, −1 + z

Bond lengths [Å]			
C1–C2/C1^{i}–C2^{i}	1.430(6)	C1–O1/C1^{i}–O1^{i}	1.226(5)
C2–C2^{i}	1.190(6)	C1–F1/C1^{i}–F1^{i}	1.281(4)
Bond angles [°]			
C1–C2–C2^{i}	179.5(5)	F1–C1–C2/F1^{i}–C1^{i}–C2^{i}	116.5(4)
O1–C1–C2/O1^{i}–C1^{i}–C2^{i}	122.1(4)	F1–C1–O1/F1^{i}–C1^{i}–O1^{i}	121.5(4)
Intermolecular contacts [Å]			
O1–(H1)···F2^{i}	2.413(4)	C2–F10^{ii}	2.794(6)
F2–(H2)···F5	2.481(5)	C1^{i}–F6^{iii}	2.871(6)
C1–F10^{ii}	2.582(6)		

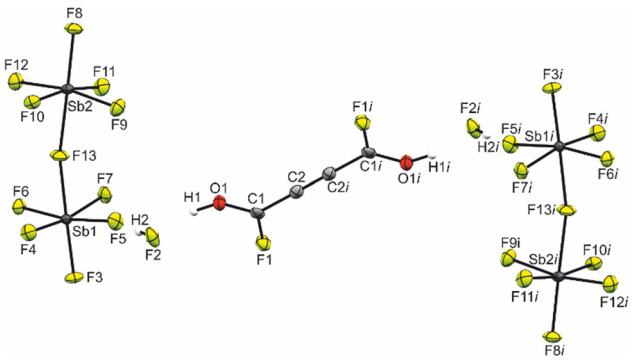

Fig. 6 Formula unit of **4** (displacement ellipsoids with 50% probability). Symmetry codes: i = 1 − x, 1 − y, 1 − z.

within the 3 σ range. The C1=O1 bond is significantly elongated by 0.048 Å to 1.226(5) Å compared to the starting material. The diprotonation shortens the C1–F1 bond by approximately 0.051 Å to 1.281(4) Å. The bond length of the $[Sb_2F_{11}]^-$ anion is in the range from 1.847(2) Å to 2.046(2) Å and agrees with those reported in the literature.[19,20] The anion is connected to the cation with hydrogen bonds *via* a co-crystallized HF molecule. According to Jeffrey, the hydrogen bonds can be classified as strong.[21] Surprisingly, in contrast to **3** and **2**, the diprotonation has a planar molecular geometry.

NMR spectroscopy

The ^{1}H, ^{13}C, and ^{19}F NMR spectra of **1** and its protonated species were measured at −50 °C in anhydrous HF (aHF) and SO_2. In Table 7 selected observed NMR shifts and couplings constants in aHF are listed. The complete data and the measured NMR spectra are given in the ESI† as well as SO_2 data. In the ^{1}H NMR spectrum, the peaks at 9.92 ppm for **2** and 9.72 ppm for **4** are the first evidence of mono- respectively diprotonation. The $^{13}C\{^{1}H\}$ NMR spectra show a trend of the shifts by protonation steps. The higher the level of protonation, the more the peak of the acid fluoride moiety is shifted downfield, and the coupling constant increases. The observation is consistent with the values reported in the literature by the protonated species of haloacetyl fluorides, CCl_2HCOF and fumaryl fluoride.[8–10] The shift downfield of cations compared to the neutral compound is reported in the literature.[8–10,22–24] The triple bond carbon atoms possess the opposite effect. The higher the protonation level, the more they are shielded, and the coupling constants decrease. In ^{19}F NMR the acyl fluoride moiety is shifted also slightly downfield by each protonation step. The change in ^{19}F NMR shift is also known from the protonation of haloacetyl fluorides, CCl_2HCOF, however is much smaller in the protonated species of $C_4O_2F_2$.[8,9] Compared to fumaryl fluoride the shifts in aHF are in the same range.[10]

Theoretical calculations

The quantum chemical calculations were performed on the MP2/aug-cc-pVTZ level of theory at 298 K using the Gaussian16 program package.[25] Further details on a comparison of calculated and measured bond lengths are shown in ESI.† The stereoelectronic features of oxygen and the supramolecular stereoelectronic effect (SSE) in carboxylic acids are well-documented in the literature.[26–28] Studies indicate that the conformation of carboxylic acids is strongly influenced by the $n_F \rightarrow \pi^*_{C=O}$ electron donation from the oxygen atom into the carbonyl group.[26] Consideration of the isolated molecule shows that the *E*-conformation is energetically less favorable compared to the *Z*-conformation.[26] As soon as hydrogen bonds can form this energetic disadvantage is reversed, making the *E*-conformation more stable than the *Z*-conformation.[26,28] Protonated carboxylic acids also show two different conformers, with the *syn–syn* and the *syn–anti* conformation.[24,29] Protonated acyl fluorides have a similar geometry compared to carboxylic acids. A few protonated acid fluorides have been published in recent years, the haloacetyl fluorides, dichloroacetyl fluoride, and fumaryl fluoride.[8–10] All five crystal structures are in the *Z*-conformation. The monoprotonated and diprotonated species of acetylenedicarbonyl fluoride also adopt the *Z* conformation. The C–F bond is shortened due to the protonation of an acyl fluoride. This shortening of the C–F bond is reported in the

Table 7 Observed ^{1}H and ^{19}F NMR chemical shifts [ppm] at −50 °C[ab]

	$C_4O_2F_2$ (**1**)	$[C_4(HO)OF_2][SbF_6]$ (**2**)	$[C_4(HO)_2F_2][Sb_2F_{11}]_2\cdot$(**4**)
^{1}H NMR		9.92(**OH**, s)	9.72(**OH**, s)
$^{13}C\{^{1}H\}$ NMR	140.2(**C**OF,d, *J* = 322.7 Hz)	141.9(**C**OF, d, *J* = 324.0 Hz)	143.7(**C**OF, d, *J* = 326.1 Hz)
	72.9(**C**≡**C**, dd, *J* = 111.9 Hz, 14.4 Hz)	72.8(**C**≡**C**, dd, *J* = 108.8 Hz, 14.3 Hz)	74.0(**C**≡**C**, dd, *J* = 104.0 Hz, 13.1 Hz)
^{19}F NMR	45.22(CO**F**, s)	45.48(CO**F**, s)	45.91(CO**F**, s)
		−120.99(s)	−120.68(s)
		−128.00(s)	−126.69(s)

[a] The observed nuclei in the assigned species are highlighted in bold characters. [b] The multiplicity of the signal is given in parentheses.

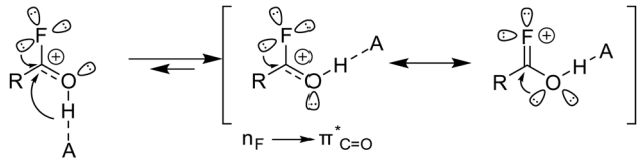

Fig. 7 The illustration of the classic *Z* effect (middle) is stronger than the supramolecular stereoelectronic effect (left). The +*R* effect stabilizes additionally due to the C–F bond shortening the *Z* conformation (right).

literature by the +*R* effect.[10] However, the +*R* effect alone is no explanation for the favoured *Z* conformation in protonated acyl fluorides. The classic *Z* effect is stronger than the SSE effect in protonated acyl fluorides (Fig. 7). The +*R* effect additionally stabilizes the classic *Z* effect.

Due to the stabilization by the classic *Z* effect and the +*R* effect the rotational barrier of the monoprotonated species of acetylenedicarbonyl fluoride is calculated. Fig. 8 displays the internal reaction coordinate (IRC) of the *E* and *Z* conformation with the transition state. The energetic accuracy for the method MP2/aug-cc-pVTZ is between 0.64 kJ mol^{-1} (mean) and 1.64 kJ mol^{-1} (maximum).[30]

The *E*- and *Z*-conformers have only a small energy gap of 2.3 kJ mol^{-1} between each other. This is in the same range as the calculated energy differences for protonated propiolic acid of 1.4 kJ mol^{-1}.[24] The energy barrier (64.8 kJ mol^{-1}) is in the same area compared to the protonated carboxylic acids formic (15.3 kcal mol^{-1} ≙ 64.0 kJ mol^{-1}), acetic (11.2 kcal mol^{-1} ≙ 49.8 kJ mol^{-1}), and propiolic acids (18.2 kJ mol^{-1}).[24,29] The not observed *E*-conformer in protonated acyl fluoride is a result of the highly temperature unstable cations. Another example for the stabilisation of conformation is the syn conformation of FC(O)SCl which is 0.31 kcal mol^{-1} (≙1.30 kJ mol^{-1}) more stable than the anti-conformer by an $lp_\pi \rightarrow \pi^*(C{=}O)$ orbital interaction.[31]

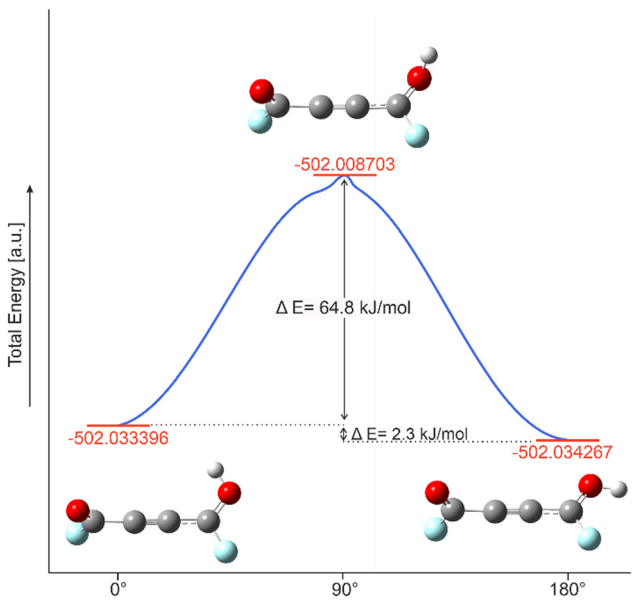

Fig. 8 IRC of the rotational barrier of the monoprotonated species of $C_4O_2F_2$ from *Z* to *E* conformation.

The system of protonated acyl fluorides would have to be exposed to very high temperatures for the thermal energy to be sufficient to enable the conformational change. The thermal decomposition of the protonated acyl fluorides is an obstacle in this process.

Conclusions

In this work, the crystal structure of $C_4O_2F_2$ is reported for the first time. Furthermore, the structure and properties of its mono- and diprotonated species are reported.[2] The diprotonated species is the first example, which is formed by the decomposition of the monoprotonation in R-134a. All compounds were characterized by single-crystal X-ray diffraction, low-temperature NMR-spectroscopy, and low-temperature vibrational spectroscopy. The experimental data are discussed together with the DFT/aug-cc-pVTZ level of theory.[32] The quantum chemical calculations in the theoretical calculations part were performed on the MP2/aug-cc-pVTZ level of theory. The theoretical calculation part explains the favoured *Z* conformation of protonated acyl fluorides. The rotational barrier is notable higher compared to the carboxylic acids.[24,29]

Experimental section

Caution! The hydrolysis of SF_4, SbF_5 $C_4F_2O_2$, and the prepared salts (2–5) might form HF which burns skin and causes irreparable damage. Safety precautions must be taken while using and handling these materials.

Apparatus and materials

All experiments were executed on an electropolished stainless-steel vacuum line. For the synthesis of acetylenedicarbonyl fluoride, 1-L-autoclaves were employed. The autoclave was dried over 1 h at 350 °C. Room- and low-temperature Raman spectroscopic studies were performed using a Bruker MultiRAM FT-Raman spectrometer with Nd: YAG laser excitation (λ = 1064 cm^{-1}) under vacuum at −196 °C. For a measurement, the synthesized compounds were transferred into a cooled glass cell. At low temperatures. IR spectra were recorded in a vacuum using a Bruker Vertex −80 V FTIR spectrometer. A small amount of the synthesized samples was placed on a CsBr single crystal plate in a cooled cell for measurement.[33] The low-temperature single-crystal X-ray diffraction of $C_4O_2F_2$ (**1**), $[C_4(OH)OF_2][SbF_6]$ (**2**), was performed on an Oxford XCalibur 3 diffractometer equipped with a Kappa CCD detector, operating with Mo-Kα (0.71073 Å) radiation (3 errors) and a Spellman generator (voltage 50 kV, current 40 mA). The program CrysAlisPro 1.171.38.46 (Rigaku OD, 2015)[34] was employed for the data collection and reduction. The structures were solved utilizing SHELXT[35] and SHELXL-2018/3[36] of the WINGX software package.[37] The structures were checked using the software PLATON.[38] The absorption correction was performed using the SCALE3 ABPSACK multiscan method.[39] Selected data and parameters of the measured single-crystal X-ray structures analyses are summarized in Table S3 (see ESI†).

NMR samples were prepared by adding the HF solution to a small FEP tube under a nitrogen stream. The tube was sealed under vacuum and inserted into a standard NMR tube. For 1H, 19F, and 13C{1H} NMR measurements a Bruker AV400TR and a JEOL ECX 400 NMR spectrometer were used. For evaluation, MNOVA by Mestrelab was used.[40] The quantum chemical calculations in the experimental section were performed on the B3LYP/aug-cc-pVTZ level of theory with the Gaussian16 program package.[25] The quantum chemical calculations were performed on the MP2/aug-cc-pVTZ level of theory at 298 K with the Gaussian16 program package.[25] For visualization and illustration of the MEP calculations GaussView 6.0 was used.[32,41]

Synthesis of acetylenedicarbonyl fluoride (1). The preparation procedure previously reported by Hasek *et al.* was optimized.[5] A dry 1-L-autoclave was filled with dried $C_4H_2O_4$ (93 mmol) in a nitrogen atmosphere. The autoclave was evacuated and SF_4 (185 mmol) was condensed in the autoclave at −196 °C. The reaction mixture was allowed to warm up to room temperature for 24 h. The product was purified by trap to trap-distillation (−78 °C and −196 °C). A colorless liquid was formed in all the experiments with a yield of around 73%. The reaction with sulfur tetrafluoride and acetylene dicarboxylic acid leads to a very pure product of acetylenedicarbonyl fluoride.

Synthesis of $[C_4(OH)OF_2][SbF_6]$ (2). Antimony pentafluoride (200 mg, 0.923 mmol,1.5 eq.) was condensed in an FEP tube reactor in a static vacuum at −196 °C. Afterward, 0.75 mL anhydrous hydrogen fluoride (aHF) was added, and the mixture homogenized at −40 °C. At −196 °C. Acetylenedicarbonyl fluoride (72.6 mg, 0.615 mmol, 1.0 eq.) was added at −196 °C to the superacidic system and warmed up to −40 °C. The solvent was removed at −78 °C overnight. The product was a white salt.

Synthesis of $[C_4(OD)OF_2][SbF_6]$ (3). Antimony pentafluoride (60.0 mg, 0.277 mmol, 2.2 eq.) was condensed in a static vacuum in an FEP tube reactor at −196 °C. Afterwards, 0.75 mL anhydrous deuterated hydrogen fluoride (aDF) was added, and the mixture homogenized at −40 °C. At −196 °C Acetylenedicarbonyl fluoride (14.8 mg, 0.125 mmol, 1.0 eq.) was condensed into the FEB tube reaction vessel. The mixture was warmed up to −40 °C. Finally, the excess solvent was removed at −78 °C overnight. The product was observed as a colorless salt.

Synthesis of $[C_4(OH)_2F_2][Sb_2F_{11}]_2{\cdot}2HF$ (4). At first (2) was synthesized. Afterward, R134a was condensed at −78 °C and after 20 min, the reaction mixture was warmed up to −25 °C for 20 min and mixed. The solvent was removed very quickly at −25 °C. The product occurs as a colorless to yellow salt.

Synthesis of $[C_4(OD)_2F_2][Sb_2F_{11}]_2{\cdot}2DF$ (5). For the synthesis of (5), R134a was added to synthesized salt (3) at −78 °C and after 20 min, the reaction mixture was warmed up to −25 °C for 20 min and mixed. The solvent was removed very quickly at −25 °C. The product was a colorless yellow salt.

Data availability

The data supporting this article have been included as part of the ESI.† For full details on vibrational spectroscopy, NMR spectroscopy, X-ray diffraction refinement, and computational details. Crystallographic data has been deposited at the CCDC under 2371787, 2371788, and 2371790.†

Conflicts of interest

There are no conflicts to declare.

Acknowledgements

We are grateful to the Department of Chemistry at the Ludwig Maximilian University of Munich, the Deutsche Forschungsgemeinschaft (DFG), the F-Select GmbH, and Prof. Dr. Karaghiosoff for their support.

Notes and references

1 T. Schirmeister, C. Schmuck and P. R. Wich, *Beyer/Walter Organische Chemie*, Hirzel Verlag, Stuttgart, 25th edn, 2016.
2 O. Diels and W. E. Thiele, Zur Kenntnis der Dien-Synthesen, XXX. Mitteil.: Über das Chlorid der Acetylendicarbonsäure, *Ber. Dtsch. Chem. Ges.*, 1938, **71**, 1173–1178.
3 G. Maier and W. A. Jung, Aktivierung von acetylendicarbonsäure durch überführung in gemischte anhydride [1], *Tetrahedron Lett.*, 1980, **21**, 3875–3878.
4 R. N. McDonald and R. A. Krueger, The Catalyzed Reaction of Acetylenedicarboxylic Acid and Thionyl Chloride, *J. Org. Chem.*, 1963, **28**, 2542–2544.
5 W. R. Hasek, W. C. Smith and V. A. Engelhardt, The Chemistry of Sulfur Tetrafluoride. II. The Fluorination of Organic Carbonyl Compounds 1, *J. Am. Chem. Soc.*, 1960, **82**, 543–551.
6 F. E. Herkes and H. E. Simmons, Acetylenedicarbonyl Fluoride, *Synthesis*, 1973, 166.
7 F. E. Herkes and H. E. Simmons, Acetylenedicarbonyl fluoride. I. Its physical properties and reaction with nucleophilic reagents, *J. Org. Chem.*, 1975, **40**, 420–423.
8 S. Steiner, A. Nitzer, C. Jessen and A. J. Kornath, Reactions of Dichloroacetyl Fluoride in Superacidic Media, *Z. Anorg. Allg. Chem.*, 2024, **650**, DOI: 10.1002/zaac.202400013.
9 S. Steiner, C. Jessen and A. J. Kornath, Synthesis and Structural Investigation of Protonated Haloacetyl Fluorides, *Z. Anorg. Allg. Chem.*, 2022, **648**, DOI: 10.1002/zaac.202200060.
10 M. C. Bayer, C. Kremser, C. Jessen, A. Nitzer and A. J. Kornath, Strengthening of the C-F Bond in Fumaryl Fluoride with Superacids, *Chemistry*, 2022, **28**, e202104422.
11 L. A. Ramos, S. E. Ulic, R. M. Romano, M. F. Erben, C. W. Lehmann, E. Bernhardt, H. Beckers, H. Willner and C. O. Della Védova, Vibrational spectra, crystal structures, constitutional and rotational isomerism of FC(O)SCN and FC(O)NCS, *Inorg. Chem.*, 2010, **49**, 11142–11157.
12 S. E. Ulic, A. Kosma, C. O. Della Vedova, H. Willner and H. Oberhammer, S-(fluoroformyl)O-(trifluoroacetyl) thioperoxide, FC(O)S-OC(O)CF3: gas-phase structure and

conformational properties, *J. Phys. Chem. A*, 2006, **110**, 10201–10205.

13 F. H. Allen, O. Kennard, D. G. Watson, L. Brammer, A. G. Orpen and R. Taylor, Tables of bond lengths determined by X-ray and neutron diffraction. Part 1. Bond lengths in organic compounds, *J. Chem. Soc., Perkin Trans. 2*, 1987, S1.

14 M. C. Bayer, C. Jessen and A. J. Kornath, Structure and Properties of Fumaryl Fluoride, *Z. Anorg. Allg. Chem.*, 2021, **647**, 258–265.

15 A. Jin, H. G. Mack, A. Waterfeld and H. Oberhammer, Gas-phase structure and conformations of malonyl difluoride (COF-CH2-COF) and difluoromalonyl difluoride (COF-CF2-COF). An electron diffraction and ab initio study, *J. Am. Chem. Soc.*, 1991, **113**, 7847–7852.

16 M. F. Erben, C. O. Della Védova, H. Willner, F. Trautner, H. Oberhammer and R. Boese, Fluoroformyl trifluoroacetyl disulfide, FC(O)SSC(O)CF3: synthesis, structure in solid and gaseous states, and conformational properties, *Inorg. Chem.*, 2005, **44**, 7070–7077.

17 R. Minkwitz, C. Hirsch and T. Berends, Synthesis and Characterisation of New Arsonium Salts and Crystal Structures of Trimethylarsonium Undecafluorodiarsenate (CH3)3AsH + As2F11− and Trimethylarsonium Hexafluoroantimonate (CH3)3AsH + SbF6−, *Eur. J. Inorg. Chem.*, 1999, 2249–2254.

18 R. Minkwitz and S. Schneider, Synthesis and Characterization of the Tetrahydroxyphosphonium Hexafluorometalates P(OH)4 + MF6− (M = As, Sb), *Angew. Chem., Int. Ed.*, 1999, **38**, 210–212.

19 J. F. Lehmann, G. J. Schrobilgen, K. O. Christe, A. Kornath and R. J. Suontamo, X-ray crystal structures of XF(6)Sb(2)F(11) (X = Cl, Br, I); (35,37)Cl, (79,81)Br, and (127)I NMR studies and electronic structure calculations of the XF(6)(+) cations, *Inorg. Chem.*, 2004, **43**, 6905–6921.

20 T. Drews, W. Koch and K. Seppelt, The Cl 2 O 2+ Cation: Preparation and Structural Investigation of Cl 2 O 2+ SbF 6- and Cl 2 O 2+ Sb 2 F 11-, *J. Am. Chem. Soc.*, 1999, **121**, 4379–4384.

21 G. A. Jeffrey, *An introduction to hydrogen bonding*, Oxford University Press, New York, Oxford, 1997.

22 D. Hollenwäger, Y. Morgenstern, L. Daumer, V. Bockmair and A. J. Kornath, Structural Investigation of Diprotonated Glycine, Diprotonated Glycine Methyl Ester, and Monoprotonated Glycinoyl Fluoride, *ACS Earth Space Chem.*, 2024, **8**, 2101–2109.

23 G. A. Olah, A. L. Berrier and G. K. Prakash, C NMR chemical shift correlations in application of ''tool of increasing electron demand'' to stable long-lived carbocations: Comprehensive evaluation, *Proc. Natl. Acad. Sci. U. S. A.*, 1981, **78**, 1998–2002.

24 D. Hollenwäger, S. Thamm, V. Bockmair, A. Nitzer and A. J. Kornath, Synthesis and Structure of Protonated Propiolic Acid, *J. Org. Chem.*, 2024, **89**, 11421–11428.

25 M. J. Frisch, G. W. Trucks, H. B. Schlegel, G. E. Scuseria, M. A. Robb, J. R. Cheeseman, G. Scalmani, V. Barone, G. A. Petersson, H. Nakatsuji, X. Li, M. Caricato, A. V. Marenich, J. Bloino, B. G. Janesko, R. Gomperts, B. Mennucci, H. P. Hratchian, J. V. Ortiz, A. F. Izmaylov, J. L. Sonnenberg, D. Williams-Young, F. Ding, F. Lipparini, F. Egidi, J. Goings, B. Peng, A. Petrone, T. Henderson, D. Ranasinghe, V. G. Zakrzewski, J. Gao, N. Rega, G. Zheng, W. Liang, M. Hada, M. Ehara, K. Toyota, R. Fukuda, J. Hasegawa, M. Ishida, T. Nakajima, Y. Honda, O. Kitao, H. Nakai, T. Vreven, K. Throssell, J. A. Montgomery Jr., J. E. Peralta, F. Ogliaro, M. J. Bearpark, J. J. Heyd, E. N. Brothers, K. N. Kudin, V. N. Staroverov, T. A. Keith, R. Kobayashi, J. Normand, K. Raghavachari, A. P. Rendell, J. C. Burant, S. S. Iyengar, J. Tomasi, M. Cossi, J. M. Millam, M. Klene, C. Adamo, R. Cammi, J. W. Ochterski, R. L. Martin, K. Morokuma, O. Farkas, J. B. Foresman and D. J. Fox, *Gaussian 16 Rev. C.01*, Wallingford, CT, 2016.

26 I. V. Alabugin, L. Kuhn, M. G. Medvedev, N. V. Krivoshchapov, V. A. Vil, I. A. Yaremenko, P. Mehaffy, M. Yarie, A. O. Terent'ev and M. A. Zolfigol, Stereoelectronic power of oxygen in control of chemical reactivity: the anomeric effect is not alone, *Chem. Soc. Rev.*, 2021, **50**, 10253–10345.

27 S. Z. Vatsadze, A. V. Medved'ko, M. K. Mirakbarov, M. E. Minyaev, V. N. Khrustalev, D. U. Zaripov, M. G. Medvedev and I. V. Alabugin, Not all carbon—carbon bonds are equivalent: anomeric effect of sp-hybridized carbon atom, *Russ. Chem. Bull.*, 2024, **73**, 363–371.

28 M. G. Medvedev, I. S. Bushmarinov and K. A. Lyssenko, Z-effect reversal in carboxylic acid associates, *Chem. Commun.*, 2016, **52**, 6593–6596.

29 H. Hogeveen, Chemistry and spectroscopy in strongly acidic solutions. Part XX: Configurational equilibration in protonated formic acid and protonated acetic acid (dihydroxycarbonium ions): (Short communication), *Recl. Trav. Chim. Pays-Bas*, 1968, **87**, 1313–1317.

30 J. Kaminsky, R. A. Mata, H.-J. Werner and F. Jensen, The accuracy of local MP2 methods for conformational energies, *Mol. Phys.*, 2008, **106**, 1899–1906.

31 M. F. Erben, C. O. Della Védova, R. M. Romano, R. Boese, H. Oberhammer, H. Willner and O. Sala, Anomeric and mesomeric effects in methoxycarbonylsulfenyl chloride, CH(3)OC(O)SCl: an experimental and theoretical study, *Inorg. Chem.*, 2002, **41**, 1064–1071.

32 M. J. Frisch, G. W. Trucks, H. B. Schlegel, G. E. Scuseria, M. A. Robb, J. R. Cheeseman, G. Scalmani, V. Barone, G. A. Petersson, H. Nakatsuji, X. Li, M. Caricato, A. V. Marenich, J. Bloino, B. G. Janesko, R. Gomperts, B. Mennucci, H. P. Hratchian, J. V. Ortiz, A. F. Izmaylov, J. L. Sonnenberg, D. Williams-Young, F. Ding, F. Lipparini, F. Egidi, J. Goings, B. Peng, A. Petrone, T. Henderson, D. Ranasinghe, V. G. Zakrzewski, J. Gao, N. Rega, G. Zheng, W. Liang, M. Hada, M. Ehara, K. Toyota, R. Fukuda, J. Hasegawa, M. Ishida, T. Nakajima, Y. Honda, O. Kitao, H. Nakai, T. Vreven, K. Throssell, J. A. Montgomery Jr., J. E. Peralta, F. Ogliaro, M. J. Bearpark,

J. J. Heyd, E. N. Brothers, K. N. Kudin, V. N. Staroverov, T. A. Keith, R. Kobayashi, J. Normand, K. Raghavachari, A. P. Rendell, J. C. Burant, S. S. Iyengar, J. Tomasi, M. Cossi, J. M. Millam, M. Klene, C. Adamo, R. Cammi, J. W. Ochterski, R. L. Martin, K. Morokuma, O. Farkas, J. B. Foresman and D. J. Fox, *Gaussian 16 Rev. C.01*, Wallingford, CT, 2016.

33 L. Bayersdorfer, R. Minkwitz and J. Jander, Eine Infrarot-Tieftemperaturkvette fr die Vermessung temperaturempfindlicher Gase, Flssigkeiten und Feststoffe, *Z. Anorg. Allg. Chem.*, 1972, **392**, 137–142.

34 *Rigaku Oxford Diffraction, CrysAlisPro Software System, Version 1.171.38.46*, Rigaku Oxford Diffraction, Rigaku Corporation, Oxford, UK, 2015.

35 G. M. Sheldrick, SHELXT – integrated space-group and crystal-structure determination, *Acta Crystallogr., Sect. A: Found. Adv.*, 2015, **71**, 3–8.

36 G. M. Sheldrick, Crystal structure refinement with SHELXL, *Acta Crystallogr., Sect. C: Struct. Chem.*, 2015, **71**, 3–8.

37 L. J. Farrugia, WinGX suite for small-molecule single-crystal crystallography, *J. Appl. Crystallogr.*, 1999, **32**, 837–838.

38 A. L. Spek, Single-crystal structure validation with the program PLATON, *J. Appl. Crystallogr.*, 2003, **36**, 7–13.

39 *SCALE3 ABSPACK, An Oxford Diffraction Program*, Oxford Diffraction Ltd, UK, 2005.

40 *MestReNova 14.0*, Mestrelab Research, 2019.

41 R. Dennington, T. A. Keith and J. M. Millam, *GaussView Version 6.0*, Shawnee Mission, KS, 2016.

